PNAS RESEARCH ARTICLE | NEUROSCIENCE OPEN ACCESS

The oxygen initial dip in the brain of anesthetized and awake mice

Ali-Kemal Aydin[a], Camille Verdier[a], Emmanuelle Chaigneau[a], and Serge Charpak[a,1]

Edited by Mark Nelson, University of Vermont, Burlington, VT; received January 5, 2022; accepted February 19, 2022

An ongoing controversy in brain metabolism is whether increases in neural activity cause a local and rapid decrease in oxygen concentration (i.e., the "initial dip") preceding functional hyperemia. This initial dip has been suggested to cause a transient increase in vascular deoxyhemoglobin with several imaging techniques and stimulation paradigms, but not consistently. Here, we investigate contributors to this initial dip in a distinct neuronal network, an olfactory bulb (OB) glomerulus most sensitive to a specific odorant (ethyl tiglate [ET]) and a site of strong activation and energy consumption upon ET stimulation. Combining two-photon fluorescence and phosphorescence lifetime microscopy, and calcium, blood flow, and pO_2 measurements, we characterized this initial dip in pO_2 in mice chronically implanted with a glass cranial window, during both awake and anesthetized conditions. In anesthetized mice, a transient dip in vascular pO_2 was detected in this glomerulus when functional hyperemia was slightly delayed, but its amplitude was minute (0.3 SD of resting baseline). This vascular pO_2 dip was not observed in other glomeruli responding nonspecifically to ET, and it was poorly influenced by resting pO_2. In awake mice, the dip in pO_2 was absent in capillaries as well as, surprisingly, in the neuropil. These high-resolution pO_2 measurements demonstrate that in awake mice recovered from brain surgery, neurovascular coupling was too fast and efficient to reveal an initial dip in pO_2.

neurovascular coupling | initial dip | oxygen

Significance

Sensory stimulation generates a robust decrease in oxygen concentration (pO_2 initial dip) in brain tissue of anesthetized cats and rodents. This dip reports local activation of neurons much better than the delayed pO_2 increase associated with functional hyperemia. Here, we reinvestigated the issue in animals that recovered from acute surgery using two-photon lifetime microscopy. Targeting a distinct neuronal network that is the site of strong activation and energy consumption, we show that in anesthetized animals the pO_2 initial dip is present but extremely small in juxtasynaptic capillaries. In awake animals, it is no longer detectable in vessels or in the neuropil. This demonstrates that in healthy animals, neurovascular coupling is too fast and efficient to reveal a pO_2 initial dip.

Functional hyperemia is the increase of blood flow triggered by neuronal activation and generated by neurovascular coupling, an ensemble of signaling pathways involving the interactions of neurons, astrocytes, endothelial cells, and mural contractile cells (1, 2). Locally activated neurons trigger a vascular signal that propagates up the vascular arbor (3–5), dilating upstream vessels with a complex temporal dynamic and resulting in a flow-velocity uncoupling at the level of penetrating arterioles (6, 7). Additionally, vascular backpropagation increases the arteriolar contribution to the brain volume irrigated by functional hyperemia (6, 8). This fixes a biological limit to the spatial resolution of all functional imaging techniques exclusively based on blood flow dynamics.

In contrast, imaging techniques such as intrinsic signal optical imaging (ISOI) or blood-oxygen-level–dependent (BOLD) functional MRI (fMRI), which report changes in deoxyhemoglobin, could potentially detect the location of neuronal activation with improved spatial resolution, as long as neuronal activation causes an increase in oxygen consumption that is measurable and precedes functional hyperemia. Early studies with ISOI reported such an initial dip, resulting from an early transient increase in deoxyhemoglobin (9) associated with rapid oxygen consumption (10). This initial dip was spatially more specific than the delayed increase of oxyhemoglobin associated with functional hyperemia. However, numerous studies did not reproduce the findings and it is now accepted that the ISOI initial dip is no longer detected when the signal analysis accounts for the wavelength-dependent pathlength in brain tissue (11–14). Similarly, although early BOLD fMRI studies reported this initial dip (i.e., negative BOLD signal) in humans (15–18) and monkey (19) and cat (20) models, it was not confirmed by others, and it is likely that a large part of the controversy relies on methodological differences, physiological conditions, and species studied (for reviews see refs. 21–25). Overall, the BOLD fMRI initial dip is not used in preclinical or clinical studies to improve the spatial resolution of activation maps.

These findings contradict the direct measurements of oxygen concentration dips reported in brain tissue of anesthetized cats and rodents. In 2003, Freeman and coworkers used paired extracellular recordings and Clark oxygen electrodes and demonstrated that in the cat visual cortex, sensory stimulation generates an initial pO_2 dip concomitant with neural firing, followed by a positive rebound (26). This strongly supported the early ISIO and BOLD fMRI dip hypothesis. Combining two-photon laser scanning microscopy (TPLSM) and a fluorescent Clark electrode targeted in a single glomerulus of the rat

Author affiliations: [a]INSERM, CNRS, Institut de la Vision, Sorbonne Université, 75012 Paris, France

Author contributions: A.-K.A. and S.C. designed research; A.-K.A. and C.V. performed research; A.-K.A. and E.C. contributed analytic tools; A.-K.A. and C.V. analyzed data; and A.-K.A. and S.C. wrote the paper.

The authors declare no competing interest.

This article is a PNAS Direct Submission.

[1]To whom correspondence may be addressed. Email: serge.charpak@inserm.fr.

This article contains supporting information online at http://www.pnas.org/lookup/suppl/doi:10.1073/pnas.2200205119/-/DCSupplemental.

Published March 30, 2022.

olfactory bulb (OB) (27), we reported that odor generates a local pO_2 initial dip in the glomerular neuropil, followed by a positive rebound due to local functional hyperemia. This tissue pO_2 dip, which started within 100 ms of neural activation, was blocked by focal application of glutamate receptor antagonists restricted to the activated glomerulus. This precisely indicated that the pO_2 dip resulted principally from postsynaptic dendritic activation rather than from firing of olfactory sensory neuron axon terminals and transmitter release. Subsequently, we used two-photon phosphorescence lifetime microscopy (2PLM) to monitor pO_2 changes in both the vascular and tissue compartments of rat and mouse glomeruli (28, 29). Although we systematically observed the pO_2 initial dip in the tissue of all responsive glomeruli, it was barely detectable in individual capillary responses. However, averaging all capillary responses and thus improving the response signal-to-noise ratio (SNR) revealed a small (≈ 1 mmHg) vascular initial dip in pO_2. Overall, direct pO_2 measurements clearly demonstrated that during natural stimulation, synaptic consumption of oxygen is immediate, systematic, local, and weakly reflected at the level of single capillaries. Such observations thus seem at odds with the "no dip" consensus in mesoscopic imaging and raise the question of whether the discrepancy is linked to the BOLD fMRI and ISIO SNR or to other parameters impacting the state of the animal, such as surgery and anesthesia, which are known to affect neuronal responses and functional hyperemia (7, 30, 31).

Here, we reinvestigated the issue in mice chronically implanted with a glass window after several weeks of recovery from craniotomy. Measurements were performed in a specific neuronal network, the olfactory bulb glomerulus most sensitive to ethyl tiglate (ET), which can be systematically targeted across animals and assumed to strongly consume oxygen. We measured changes of neural Ca^{2+} and capillary velocity with TPLSM and monitored pO_2 in glomerular capillaries and neuropil with 2PLM and the oxygen sensor Oxyphor 2P (32). Our results show a detectable dip in vascular pO_2 in only ≈ 50% of anesthetized mice, and no dip in capillary and tissue pO_2 in awake animals. These data reconcile high-resolution measurements of pO_2 with ISIO and BOLD fMRI in response to natural sensory stimulation.

Results

pO_2 Responses in Capillaries of Anesthetized Mice Supplemented with Oxygen. We focused our work on the olfactory bulb glomerulus most sensitive to ET in mice chronically implanted with a glass cranial window. Mice were anesthetized (*Methods*), supplemented with oxygen, and without correction of the objective temperature, thus consistent with the experimental conditions where the initial dip in vascular pO_2 was previously observed (with the exception of recovery from surgery) (29). Note that imaging with a water immersion objective lowers brain surface temperature to about 33 °C in anesthetized mice (33), decreasing resting blood flow and slowing down functional hyperemia (34), two effects that improve the probability of detecting an initial dip. The glomerulus most sensitive to ET was systematically found in the vicinity of the M72 glomerulus, which expresses YFP under the M72 promoter in the mouse strain used (35). Fig. 1*A* illustrates that by lowering the ET concentration to the range of 0.02%, this glomerulus was the only glomerulus showing a fast Ca^{2+} response from mitral cell dendrites. Intravenous injection of fluorescein coupled with linescan acquisitions further confirmed ET-generated, concentration-dependent Ca^{2+} and red blood cell (RBC) velocity responses in this glomerulus (Fig. 1*B*). To account for the jitter in odor onset that occurs during natural breathing, we aligned all Ca^{2+} responses such that neuronal responses started at 10 s in all our data. RBC velocity measurements were also time shifted according to Ca^{2+} response onsets as they were acquired simultaneously with the linescans (36). In contrast, oxygen measurements are done with point acquisitions targeted in the capillary center, thus theoretically without excitation of GCaMP6 expressed in pericapillary dendrites. However, we took advantage of the point-spread function (PSF) of our setup (28), which is enlarged in brain tissue (37) and thus larger than the capillary diameter (29) to measure simultaneously pO_2 vascular responses and pericapillary calcium responses (Fig. 1*C*). This allowed us to align pO_2 and flow responses to the onset of neuronal responses. Fig. 1*D* illustrates that odor triggered a concentration-dependent increase in pO_2, even at low ET concentration (same capillary as in Fig. 1*B*). No obvious initial dip was detected prior to increase in pO_2, even when averaging the responses from all mice (Fig. 1*E*) or when comparing pO_2 values immediately after neuronal activation (see the first three bins preceding pO_2 increase, Fig. 1*F*).

Due to vessel-to-vessel heterogeneity in RBC flux, which drives variability in pO_2, we normalized our time series by the noise of the baseline (first 10 s) and plotted traces as Z-scores (Fig. 2 *A*, *Bottom*). To detect whether the dip was present on average we bootstrapped the baseline values and computed a 95% CI (*Methods*). The initial dip location was chosen as the period between 0.5 and 1.5 s after the stimulus as previously observed (29). In the response averaged over all mice at a rather high concentration (ET 6%), we found that there was an initial dip with a mean value of 0.3 SD (Fig. 2*A*). By focusing on individual mice, we found that 7 of the 14 mice exhibited the initial dip (Fig. 2*B*). In capillaries where individual RBCs were well detected with point measurements, we observed a delay of 1 s between flow and pO_2 onsets (Fig. 2*C*). Interestingly, mice in which an initial dip was detected also were found to have a greater flow delay (1.2 to 1.6 s), i.e., delayed functional hyperemia. *SI Appendix*, Fig. 1 shows that using our previous approach to detect erythrocyte-associated transients (EATs) in capillaries (29, 33, 38), the initial dip observed in the trace of pO_2 mean (collecting all decays, Fig. 2 *A* and *B*) reflects what occurred at the level of pO_2 inter RBC, the pO_2 measured between two RBCs. *SI Appendix*, Fig. 1*D* also shows that the capillary initial dip is independent of resting pO_2 Mean or pO_2 Inter RBC.

These data show that, following ET exposure, the pO_2 initial dip is present but small (≈ 0.3 SD) in capillaries of the glomerulus most sensitive to ET. Can this observation be extended to other glomeruli, as at high odor concentration all odorant receptors lose their specificity and several responding glomeruli are distributed over the entire dorsal OB (39)? Each dorsal olfactory bulb (n = 4 mice) was divided into six areas and responses were recorded from one glomerulus per area (Fig. 3 *A* and *B*). In these nonspecific glomeruli, 6% ET triggered calcium, RBC velocity, and pO_2 responses that were widely variable (22 glomeruli), but the average pO_2 response did not show any indication of an initial dip in vascular pO_2 (Fig. 3*C*), suggesting that the initial pO_2 dip detected is exclusive to capillaries in the glomerulus most sensitive to the odor used (ET).

Removal of Oxygen Supplementation. Mild acute hypoxia modulates neurovascular coupling (40, 41) and cerebral blood flow (CBF) according to the brain region (42). We thus tested whether decreasing the percentage of oxygen inhaled could enhance the initial dip. We sequentially measured neuronal and vascular responses to ET 6% with and without oxygen

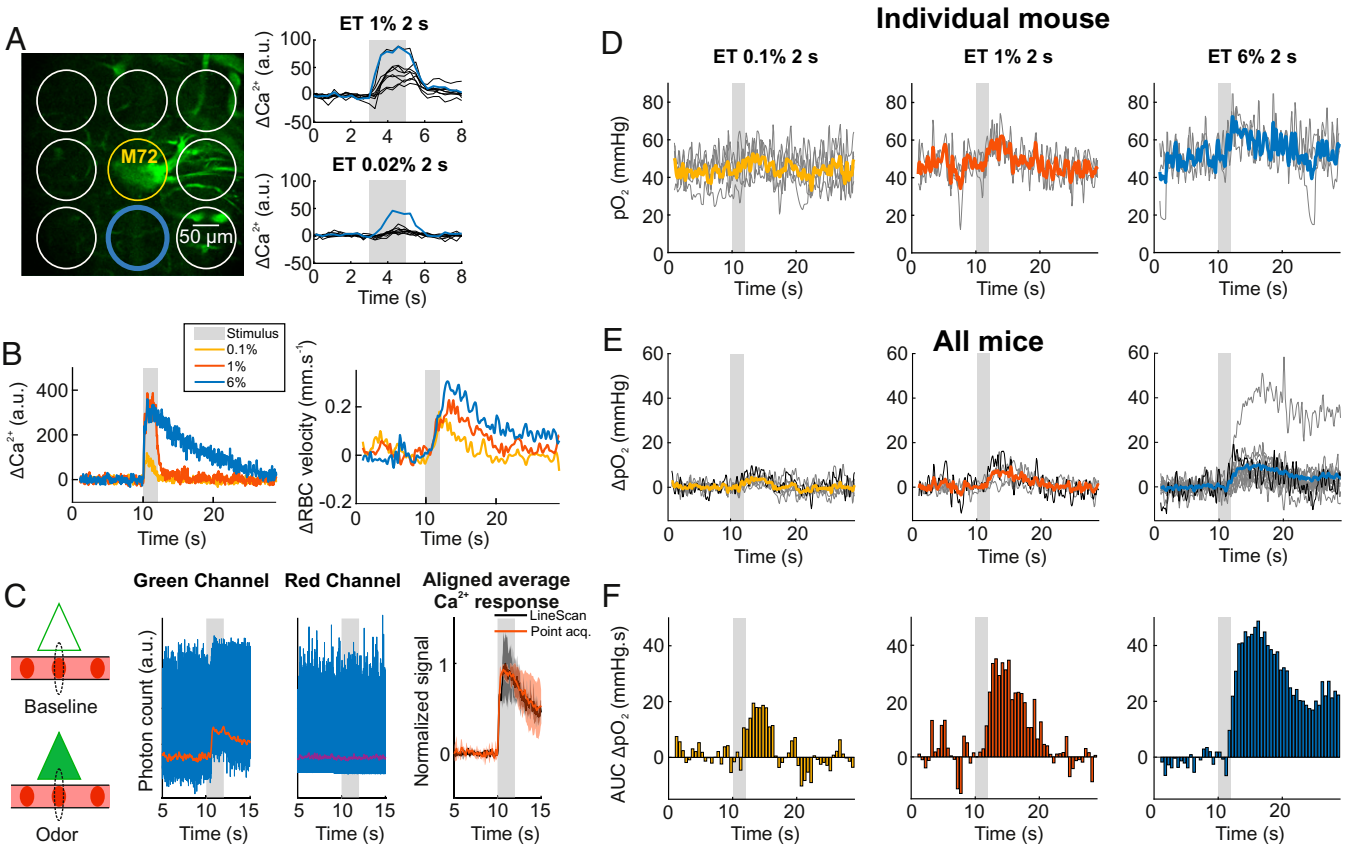

Fig. 1. pO_2 dynamics in capillaries of the olfactory bulb glomerulus most sensitive to ethyl tiglate (ET). (*A*) The most sensitive glomerulus to ET (blue circle), which is located in the vicinity of the M72 glomerulus (yellow circle) in which converge olfactory sensory neuron axons expressing YFP. The most sensitive glomerulus (blue trace) is the only one that responded to 0.02% ET concentrations. Ca^{2+} signals were collected within circles (single trials). (*B*) Typical neural (Ca^{2+}) and vascular (RBC velocity) responses acquired simultaneously with a broken linescan traced through a capillary and the neuropil in the most sensitive glomerulus (same as in *A*). Responses increased with ET concentration (0.1%, 1%, and 6%, averages of two acquisitions). (*C*) Ca^{2+} measurements during pO_2 point acquisitions. In the brain, the point-spread function (PSF, dotted black line) of our two-photon microscope is slightly larger in Z than the diameter of small capillaries. A point acquisition targeting the capillary center will excite juxtacapillary GCaMP6 dendrites (triangles). This allows for the monitoring of Ca^{2+} responses (green channel, *Left*) during the acousto-optic modulator ON period. Note that the signal from the phosphorescence in the red channel (Oxyphor 2P) remains constant (*Middle*). Normalized average responses from point (orange) and linescan (black) acquisitions are superimposable ($R^2 = 0.97$); shade is ±1 SD (*Right*). (*D*) Single (thin gray) and averaged (thick colored) pO_2 responses to increasing odor concentration in a single capillary (same as in *B*). Averages of five, three, and three trials for ET 0.1%, 1%, and 6%, respectively. (*E*) pO_2 responses to increasing odor concentrations in this glomerulus for all animals. Individual averages (thin gray) and mean of all averages (thick traces) for ET 0.1%, 1%, and 6% (n = 6, 4, and 14 mice, respectively). Thin black traces are the same as in *D*. (*F*) Binning histograms for the three means (area under the curve [AUC], bin of 0.5 s). All experiments were performed during anesthesia.

supplementation in air inhaled by anesthetized, freely breathing mice. Fig. 4 illustrates a case where removing oxygen supplementation changed resting vascular parameters, which stabilized within ≈ 15 min: all pO_2 values decreased (pO_2 Mean, RBC pO_2, and pO_2 Inter RBC), whereas RBC velocity and flow increased. In addition, it reduced functional hyperemia and canceled or suppressed odor-evoked increase in pO_2, without changing the neuronal response. The consequences of oxygen removal were robust in all mice (Fig. 4 *B*–*E*). Interestingly, onset of RBC velocity and flow responses (Fig. 4*E*) remained stable. Averaging the responses from all mice (Fig. 4*F*) showed that, whereas neuronal response dynamics were not sensitive to the drop of resting pO_2, RBC velocity and flow responses slowed down slightly. Finally, applying the same procedure as in Fig. 2 revealed that removing O_2 supplementation increased the pO_2 initial dip, but only by 0.14 SD (Fig. 4*G*). These data show that the initial dip remains small and hidden in the noise. In addition, as resting pO_2 Inter RBC reports pO_2 in the juxtacapillary neuropil (29), oxygen supplementation removal shows that neural responses were not affected by a 50% drop in resting pO_2 in the tissue. They were also insensitive to the drop of hemoglobin saturation from 73 to 42% as estimated from pO_2 RBC values in both conditions (*Methods* and ref. 38).

pO_2 Responses in Vessels and Tissue of Awake Head-Fixed Mice. As anesthetics are widely known to affect neural activity, functional hyperemia, and general body homeostasis, we tested for the presence of the initial dip in this same glomerulus (olfactory bulb glomerulus most sensitive to ET) and the neighboring glomeruli of awake mice (n = 16 glomeruli, three mice) habituated to head restraint and odor delivery for more than 2 wk (6). Fig. 5 shows a stable acquisition during which RBC flow was measurable simultaneously with pO_2. Averaging pO_2 responses from all capillaries did not reveal any initial dip prior to pO_2 increase (Fig. 5 *B*, *Bottom*, blue trace). To investigate for the presence of the dip in the glomerular tissue, some capillaries in which vascular pO_2 was first measured were then scanned for 1 to 2 prolonged periods (30 s each) at a high laser power (920 nm, > 100 mW). This altered the blood brain barrier generating transient leaks of Oxyphor 2P in the juxtacapillary region (n = 3) or even ruptures (n = 6). Point measurements of pO_2 and calcium were then immediately performed in the tissue adjacent to the capillary wall. Neural responses were maintained and systematically associated with pO_2 increases in the neuropil (Fig. 5 *B*, *Top*). Tissue pO_2 responses indicate that oxygen was still delivered by the leaking/breached capillary and the neighboring capillaries. Importantly, they

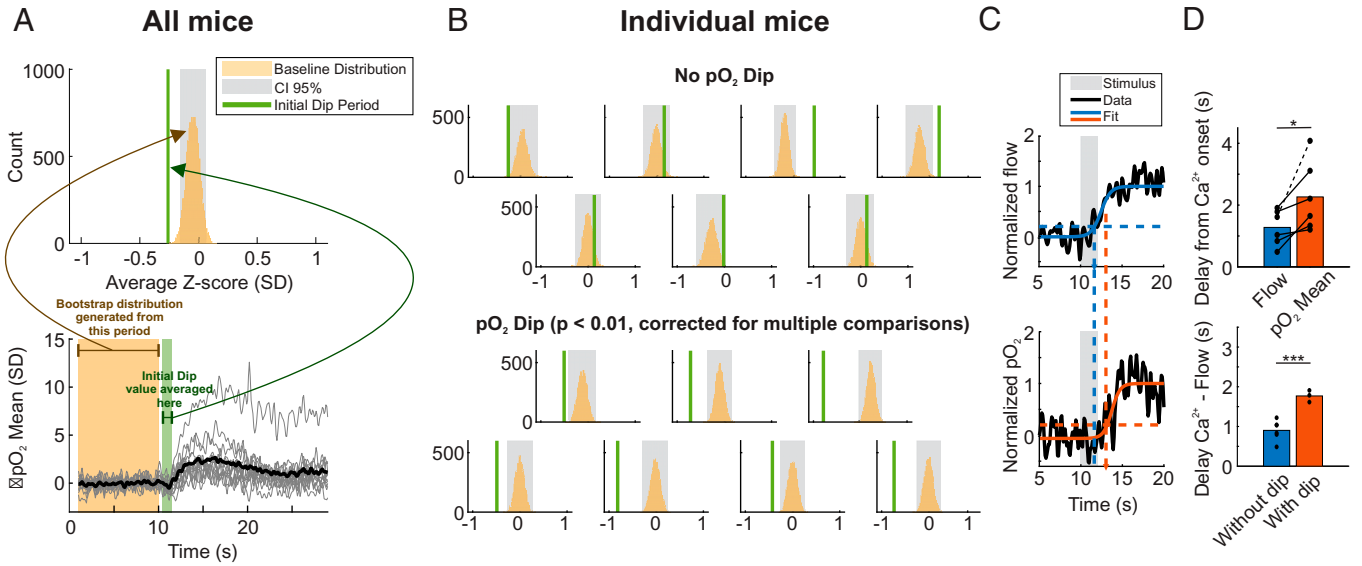

Fig. 2. A small capillary initial dip is visible when functional hyperemia is delayed. (*A*) Statistical analysis of the mean of all pO_2 responses. *Bottom*, the same traces as in Fig. 1*E*, but in Z-score (the SD was determined on the baseline). The black trace is the mean of all response averages (n = 14 mice). Generating a bootstrap distribution (*Top*) of the baseline values (black trace) shows that the initial dip, calculated as the average value of the signal between 10.5 and 11.5 s, is out of the 95% CI of the baseline distribution (*Methods*) but is small (0.26 SD, n = 14 mice, P = 0). (*B*) Statistical analysis for all individual mice. An initial dip is observed only in 50% of glomeruli (*Lower* two lines, one-sided test) (*Methods*). (*C*) Flow (*Top*) and pO_2 (*Bottom*) onsets are determined by fitting a sigmoidal curve (colored line) and selecting the 20% value of the normalized trace. (*D*) *Top*, the flow response precedes the pO_2 response by a delay of ≈ 1 s (P < 0.02, one-sided Wilcoxon signed rank test). *Bottom*, the dip is present when the delay between Ca^{2+} and flow responses is large. Note that only mice in which a Ca^{2+} response could be simultaneously acquired with RBC flow were considered (n = 3 mice with a dip, and n = 6 without a dip, P < 0.001, one-sided two-sampled t test). *P < 0.05, ***P < 0.001. All experiments were performed during anesthesia.

were never preceded by any detectable transient decrease in pO_2 (Fig. 5 *B*, *Bottom*), calling into question the existence of the pO_2 initial dip in awake mice.

Discussion

The goal of our study was to explain the discrepancy between the accepted absence of deoxyhemoglobin initial dips by the ISIO and BOLD fMRI communities and the pO_2 dips previously reported with Clark electrodes and 2PLM measurements (26–29, 43–45). As these pO_2 dips had been observed in acutely prepared anesthetized mice, rats, or cats, we tested the hypothesis that the initial dip would be different in animals fully recovered from surgery, whether anesthetized or awake.

The olfactory bulb glomerulus is an ideal neurovascular model to investigate the pO_2 dip: the neuronal network receives about 90,000 terminals synapsing on mitral and juxtaglomerular dendrites in a confined volume (mean diameter 100 μm) (46). The vast majority of these cells establish dendrodendritic synapses within the glomerulus. As a result, odor stimulation causes a huge release of neurotransmitters and a strong dendritic activation, which plays a major part of the local consumption of oxygen (27). This oxygen consumption, which was detected in each responsive glomerulus from acutely prepared rats and mice (27–29), should be enhanced in the glomerulus most sensitive to a given odorant molecule. Here, our data show that in anesthetized mice with a chronic glass window, 1) a minute dip in vascular pO_2 was observed in only 50% of glomeruli most sensitive to ET across individual animals, independently of resting capillary and tissue pO_2; 2) it occurred in glomeruli in which functional hyperemia was slightly delayed, consistent with what has been observed in

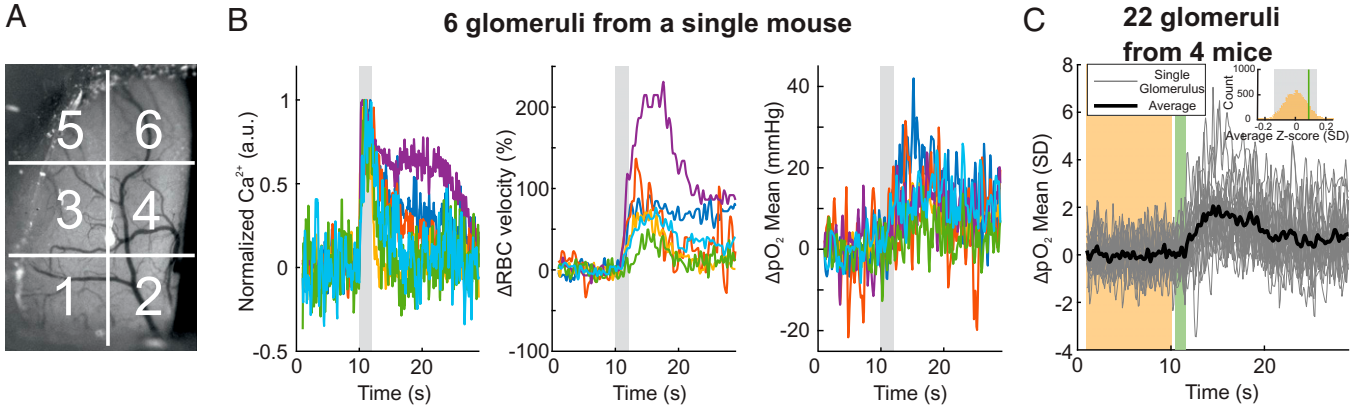

Fig. 3. Nonspecific glomeruli do not show any capillary initial dip. (*A*) Image acquired with a stereoscope through the chronically implanted window. Each olfactory bulb was divided into six regions. One glomerulus responding to 6% ET was selected in each region. (*B*) Neural and vascular responses to 6% ET for each glomerulus. (*C*) As in Fig. 2*A*. The *Inset* shows that the bootstrap CI contains the initial dip period (P = 0.9). All experiments were performed during anesthesia.

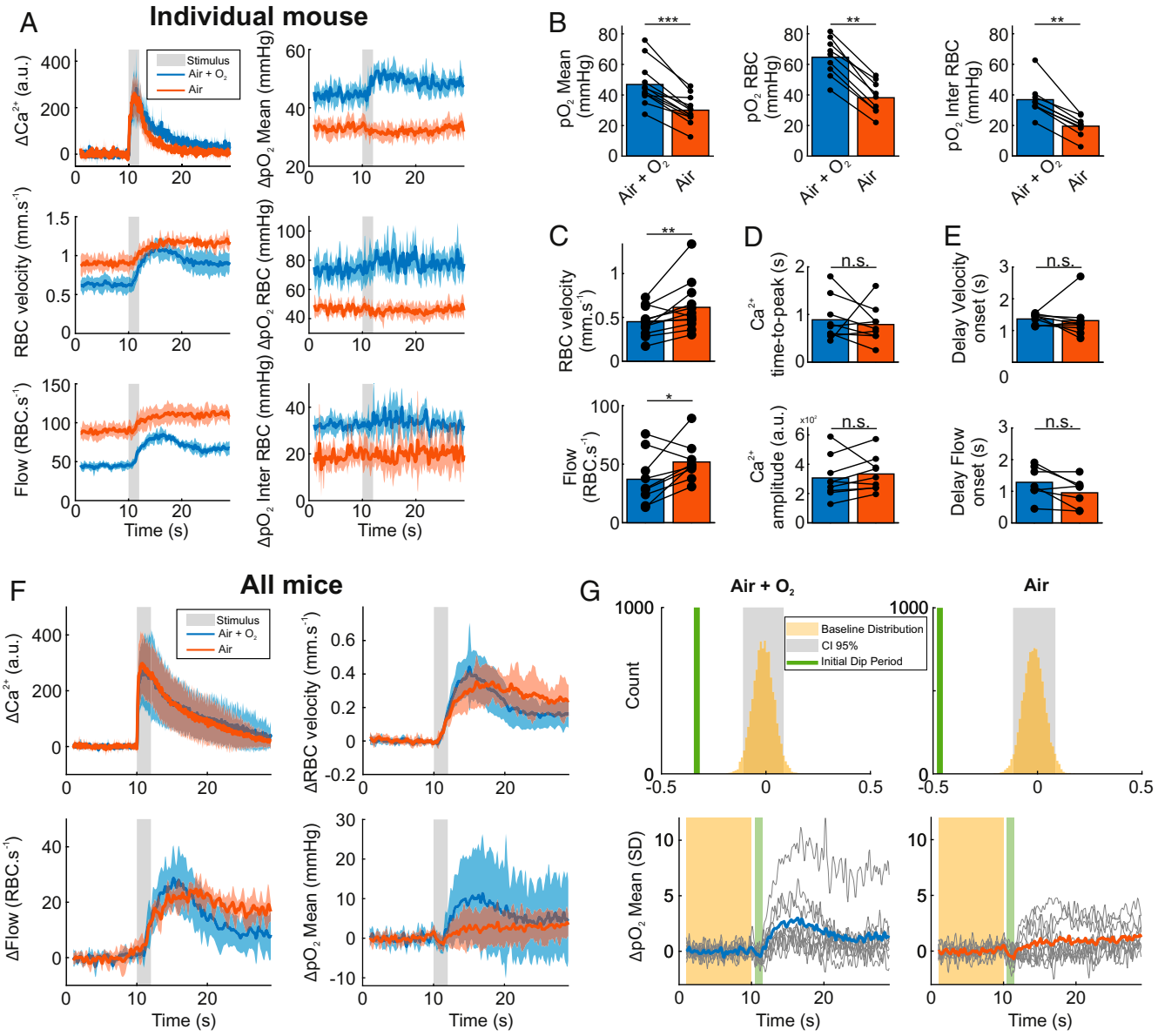

Fig. 4. Reducing the level of oxygen inhaled correlated with a slight increase in the capillary pO_2 initial dip. (*A*) Reducing the oxygen inhaled from 37 to 21% resulted in decreased resting pO_2 mean, pO_2 RBC, and pO_2 inter RBC, whereas it resulted in increased resting RBC velocity and flow. It also reduced flow and RBC responses to ET (6%, 2 s) and canceled pO_2 responses (thick line, mean ±1 SD, shaded area). Note that neural responses remained mostly constant. (*B*) Summary bar graphs for all pO_2 resting values (one-sided Wilcoxon signed rank test, $P < 0.001$, $P = 0.002$, $P = 0.002$). (*C*) Summary bar graphs for all resting RBC velocity and flow values (one-sided Wilcoxon signed rank test, $P = 0.005$, $P = 0.02$). (*D*) Oxygen reduction did not affect Ca^{2+} response time peak and amplitude (two-sided Wilcoxon signed rank test, $P = 0.36$, $P = 0.2$, *Top* to *Bottom*). (*E*) Oxygen reduction did not affect flow and velocity onsets (two-sided Wilcoxon signed rank test, $P = 0.4$, $P = 0.11$, *Top* to *Bottom*). (*F*) Evoked responses for all mice (thick line, mean ± 1 SD, shaded area). (*G*) The initial dip (*Left*, control as in Fig. 2*A*) is slightly enhanced upon reduction of the oxygen inhaled (*Right*, $n = 10$ mice). "n.s." represents not significant, $^*P < 0.05$, $^{**}P < 0.01$, $^{***}P < 0.001$. All experiments were performed during anesthesia.

humans (47); 3) it is exclusive to the glomerulus identified as the glomerulus most sensitive to ET; 4) it is about 0.3 SD of resting pO_2, whereas the peak pO_2 response reached 2.5 SD of resting pO_2, explaining why the dip is not easily detected under standard BOLD fMRI conditions; and 5) it is modestly enhanced (0.34 SD to 0.47 SD) upon removal of oxygen supplementation used to compensate for an anesthesia side effect. Note that oxygen removal caused a significant decrease in all resting pO_2 values. pO_2 Inter RBC decreased by 50%, without affecting neuronal responses, indicating that neurons have more than enough oxygen to maintain a proper short-term function. pO_2 RBC also dropped, with a decrease in resting hemoglobin saturation from 73 to 42%. Such an effect would shift the site of low hemoglobin saturation from the venous site to the capillary bed, a phenomenon that must be taken into consideration with BOLD fMRI during hypoxia.

In glomeruli of awake mice, the pO_2 dip was not detected in the tissue. This latter result is important, since detection of a pO_2 dip in tissue could be used as a readout of local neural activation, in particular with high-field BOLD fMRI (48). It is most likely that the absence of a detectable pO_2 dip in tissue depends on the dynamics of neurovascular coupling. Using anesthetized and acutely prepared animals, Kim and coworkers reported that the BOLD fMRI dip is not observed in the rat cortex upon forepaw stimulation (49), whereas it was well detected in the cat visual cortex (20). This clearly stressed the risk of comparing results from different species or brain regions, under different anesthetics. In awake animals, CBF responses

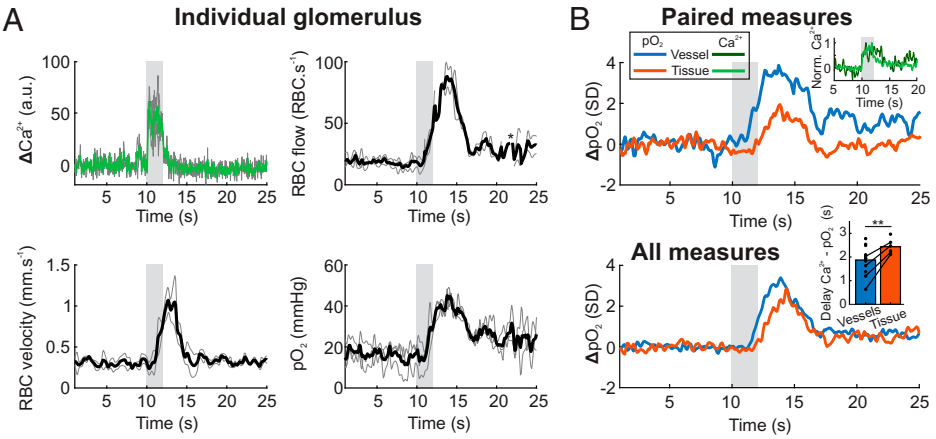

Fig. 5. The pO_2 initial dip is not detected in capillaries or in the tissue of awake mice. (*A*) Responses to ET in a glomerular capillary. *Left*, Ca^{2+} and RBC velocity are acquired simultaneously with a linescan ($n = 2$ trials) prior to a pointscan acquisition of pO_2 and RBC flow (*Right*, $n = 3$ trials). No initial dip was visible in the pO_2 response. The * in the flow trace indicates that some outlier data points were removed due to movement (*Methods*). (*B*) *Top*, pO_2 and Ca^{2+} responses were acquired before (blue and dark green traces, respectively) and after thermal lesion of the blood brain barrier (orange and light green traces, $n = 4$ glomeruli, 2 mice). *Inset*: Ca^{2+}responses remain identical before and after the thermal lesion. *Bottom*, Average pO_2 responses revealed no initial dip in capillaries ($n = 16$ glomeruli, 3 mice) or in the neuropil ($n = 9$ glomeruli, 2 mice). *Inset*: In the tissue, the pO_2 increase is delayed (one-sided paired *t* test, $P = 0.006$, one-sided two-sampled *t* test, $P = 0.025$). $^{**}P < 0.01$.

are faster than during anesthesia (31, 50). Monitoring both local neuronal activity and functional hyperemia, we have recently quantified that in the barrel cortex, neurovascular coupling and its modeled transfer function are about two times faster in awake mice than in anesthetized mice implanted with a chronic window (7). As this finding is not observed in the olfactory bulb (51), it is difficult to extrapolate whether the absence of the vascular pO_2 dip recently reported in the neocortex (51) is also supported by an absence of a pO_2 dip in the tissue.

To conclude, our precise 2PLM measurements of pO_2 demonstrate that the initial dip previously reported in tissue most probably resulted from an altered homeostasis vascular state due to acute surgery and general anesthesia. In animals anesthetized but having recovered from surgery, the initial dip is still present but almost negligible. It was no longer detectable in awake animals even when precisely targeting a brain site that undergoes a strong synaptic activation. Neurovascular coupling in healthy control animals is thus too fast and efficient to reveal a dip in oxygen concentration, at least with the temporal resolution currently achievable, for use as a proxy to improve mesoscopic functional imaging. On the other hand, one would expect to unmask this initial dip in diseases altering neurovascular coupling, such as small vessel diseases.

Methods

Animal Preparation. All animal care and experimentations were performed in accordance with the INSERM Animal Care and Use Committee guidelines (protocol nos. CEEA34.SC.122.12 and CEEA34.SC.123.12). Adult mice (3 to 12 mo old, 20 to 35 g, both males and females, housed in a 12-h light/dark cycle at 24 °C and 50% humidity, fed ad libitum) were used in this study. Thy1-GCaMP6f (GP5.11) mice (52), from The Jackson Laboratory, were crossed with M72→S50-IRES-hChRVenus mice (35) kindly provided by Thomas Bozza, Northwestern University, Evanston, IL. All mice underwent a surgery composed of the placement of a headbar on the bone behind the craniotomy, above the olfactory bulbs. Anesthesia was performed with an intraperitoneal (IP) bolus of ketamine (100 $mg{\cdot}kg^{-1}$ body mass) and medetomidine (0.4 $mg{\cdot}kg^{-1}$ body mass). To prevent inflammatory reaction and avoid infections, enrofloxacine (Baytril 10%, Bayer) and dexamethasone (Dexazone, Virbac) were administered 1 h before the surgical procedure, respectively, at 5 $mg{\cdot}kg^{-1}$ and 6 $mg{\cdot}kg^{-1}$ body mass. During surgery, mice breathed oxygen-supplemented air (60% oxygen) and body temperature was maintained at 36 ± 0.5 °C using a rectal probe and a heating pad. The headbar was first placed with Tetric Evoflow dental cement (Ivoclar Vivadent AG) after treating the bone with a primer, Optibond FL (Kerr Italia SRL). The bone above the olfactory bulbs was carefully drilled and removed, while making sure no pressure was applied on the brain tissue and heat regularly dispersed by means of using a cool artificial cerebrospinal fluid solution. A cranial window cut out of glass was placed over the bare olfactory bulbs and sealed in place with the same dental cement as used for the headbar. Buprenorphine (Buprecare, Axience) was injected to relieve pain at 0.05 $mg{\cdot}kg^{-1}$ body mass. At 3 d of postsurgery, a followup was systematically performed to monitor the animals and ensure healthy recovery. Animals were allowed to recover for more than 1 wk before starting experimental procedures.

Experimental Procedure under Anesthesia. Mice were anesthetized with a mixture of ketamine–medetomidine (100 $mg{\cdot}kg^{-1}$ and 0.4 $mg{\cdot}kg^{-1}$, respectively) injected IP. Dextran fluorescein (MW = 70 kDa, D1823, Thermo Fisher) and Oxyphor 2P (53) (5 μM in the mouse blood) was injected intravenously via retroorbital injection. Mouse temperature was monitored as during the surgery and the mouse breathed a mixture of air supplemented with oxygen (37% oxygen), except in experiments shown in Fig. 4 where the supplementation was removed (21% oxygen).

Odor Stimulation. All experiments were performed with the same stimulation protocol, so no blinding was involved. Odor delivery followed a similar procedure as in previous studies (54, 55). Odors were delivered with a home-built olfactometer controlled by custom LabVIEW software. Odor and exhaust lines were systematically equilibrated before each experiment to avoid pressure artifacts. Odor concentration and stability over the stimulus were assessed and calibrated using a photoionization detector (miniPID 200B, Aurora Scientific). To check for anesthesia-related variations during the experiment, the different stimulus conditions were randomly interleaved by the experimenter. In Fig. 5 only, linescans were performed only once per glomerulus to detect all responsive glomeruli over the bulb. This was followed by repetitive oxygen measurements in individual capillaries. Odor applications were separated by a 3-min period to allow full neuronal and vascular recovery (56).

TPLSM Acquisition. TPLSM imaging was performed with a custom-built microscope, previously described (33, 38) and data were collected with custom LabVIEW software (National Instruments). Laser pulses at 120 fs were delivered by a Ti:Sapphire laser (Mira by Coherent, 76 MHz). Laser power was modulated with an acousto-optic modulator (AA Optoelectronic, MT110B50-A1.5-IR-Hk). Galvanometric mirrors (Cambridge Technology) were used to target the sample at the desired points. Light was focused onto the sample through either a 40× W 0.8 numerical aperture (NA) or 60× W 1.1 NA objective (Olympus). GCaMP6f,

fluorescein dextran and Oxyphor 2P were excited at 920 nm and their emission was separated from the excitation light with a dichroic mirror (DXCR 875, Chroma Technology Corp [Chroma]). Emitted photons were divided by a dichroic mirror (cutoff wavelength = 560 nm). The green channel was shortpass and bandpass filtered (E800 and HQ 525/50 nm, Chroma Technology Corp). The red channel had one lowpass filter (E800, Chroma), one bandpass filter (FF01 794/160, Semrock), and a red-sensitive photomultiplier tube (R6357, Hamamatsu).

Linescan acquisitions through vessels and tissue were performed by scanning with a broken line (1 to 2.5 ms per line) for 30 s (36). The first line segment was run through the capillary (RBC velocity measurements), whereas the rest of the line scanned through the parenchyma (Ca^{2+} measurements).

Point acquisitions were performed either in a capillary or in the tissue (Fig. 5). In the capillary, it allowed us to measure simultaneously the RBC flow and pO_2. Each scan is composed of an ON period, lasting for 25 μs, where the point is excited by light at 920 nm, and an OFF period, lasting for 225 μs. RBC flow was extracted from the ON period in the green channel, thanks to fluorescence variations related to each RBC. pO_2 was extracted from the OFF period, by estimating the decay of phosphorescence in the red channel and converting the half-life of the decay to an absolute value of partial pressure of oxygen in millimeters of mercury (32). Note that our experiments were done at brain temperatures of ≈ 33 °C and 35 °C (when mice were anesthetized or awake, respectively) (33) and that the corresponding calibration curve between half-life and pO_2 was used. A single point of pO_2 in our time series is the result of the average decay over 250 ms, i.e., 1,000 decays for pO_2 Mean. Note that as pO_2 RBC and pO_2 Inter RBC measurements are extracted on the same time scale, but by averaging only the decays around RBCs or in between RBCs, the number of averaged decays is smaller for each point. Due to this lower number of decays, the signal-to-noise ratio of pO_2 Inter RBC measurements is lower and some obvious out-of-range points (>100 mmHg change for a single point) were removed (only six points for all acquisitions).

Linescan Data Analysis. Raw calcium time series were downsampled to $\Delta t = 50$ ms (*interp1* function, "pchip" option, MATLAB 2018a) and aligned so that their onset was at 10 s. After alignment, single acquisitions were normalized by subtracting the mean baseline value, and acquisitions were then averaged per trial and per mouse.

RBC velocity extraction from the linescan acquisition was done with custom LabVIEW software, with a point every 300 ms. RBC velocity was also aligned to the onset of the calcium response using the simultaneously acquired calcium trace. Each time series was then upsampled to $\Delta t = 100$ ms. Normalization was done by subtracting the mean baseline value to get the ΔRBC velocity time series in $mm{\cdot}s^{-1}$. Fig. 4 shows ΔRBC velocity time series in percent of changes, where the previous time series were divided by the same baseline value. Acquisitions were then averaged per trial and per mouse.

Point Acquisition Data Analysis. Time series from point acquisitions were aligned to the calcium onset of the simultaneously acquired calcium response, as described in Fig. 1 and the next section. Each trace was aligned so that the neuronal response starts at 10 s.

Raw RBC flow and pO_2 Mean, pO_2 RBC, or pO_2 Inter RBC were first aligned and then upsampled to $\Delta t = 100$ ms. Average baseline values before the stimulus onset were subtracted to normalize the time series, before per trial, per animal averaging. Z-score traces were computed using the normalized acquisition and by dividing the trace by the average baseline SD (*std* function, MATLAB 2018a). Z-score acquisitions were then averaged per trial and mouse.

Alignment of Data from Point Acquisitions. To align pO_2 point acquisitions to neuronal responses, we used calcium responses from dendrites expressing GCaMP6f in the pericapillary parenchyma. As the radii of capillaries are slightly smaller than the microscope PSF in Z, in situ (28, 37), the green fluorescence channel collects fluorescence from plasmatic fluorescein and from dendrites (Fig. 1*C*). To extract calcium responses, we collected green fluorescence at the imaged point during the passage of each RBC. At this point, plasma fluorescence varied from a minimum value ("darkness" collected at the RBC center) to a maximum value (between two RBCs). Calcium response was collected only when plasma fluorescence was below 30% of the maximum value (i.e., during RBCs) to decrease the weight of plasma "pollution." Fig. 1*C* shows that we can faithfully recover the calcium response dynamics while keeping a steady trace in the red channel. Time shift for the alignment was defined for each acquisition by the experimenter, as for the linescans.

Vascular Onset Computation. As shown in Fig. 4, vascular onsets were determined by fitting traces with a sigmoid function (MATLAB 2018a). The time to 20% of the peak of the fit was used to calculate the onset of either RBC velocity, RBC flow, or pO_2. Each fit was hand checked by the experimenter to make sure that the fits were faithful.

Statistical Analysis. Comparison between paired onset delays (Figs. 3 and 4) was performed with a one-sided Wilcoxon test (*signrank* function, MATLAB 2018a), as we did not assume a normal distribution and we looked for a dip. Regarding comparisons where no assumption was made, namely Ca^{2+} amplitude and onset together with vascular delays (Fig. 4 *D* and *E*), a two-sided Wilcoxon test was performed (*signrank* function, MATLAB 2018a).

To determine whether there was a dip in the response of individual animals, or in the mean response of all mice, we performed a bootstrap test (Figs. 2, 4, and 5) to compare the noise of baselines and responses. A bootstrap distribution of the average value of the baseline (in Z-score) was determined by the following procedure: for a given mouse, we 1) considered the values from all trial baselines (40 points per baseline × trial numbers); 2) randomly selected 40 points and determined the average; 3) reshuffled the 40 points selected 10,000 times; and 4) generated a 95% CI based on the distribution of the average baseline values. A significant dip was then defined by the average value of the dip, computed as the mean response between 10.5 and 11.5 s (*Results*), being smaller than the lower threshold of the CI. The *P* value of the test was determined as the number of baseline values smaller than the average dip value, divided by 10,000. The baseline distribution was generated by considering the time points before the stimulus onset (first 10 s prior to the odor). All traces were in Z-scores.

Data Availability. All data have been deposited as MAT files on Zenodo and is publicly accesible at https://doi.org/10.5281/zenodo.5804933 (57). Code used to generate figures is available on GitHub at https://github.com/alike-aydin/InitialDip_AydinEtAl (58).

ACKNOWLEDGMENTS. We particularly thank Manon Omnes who performed all mouse surgeries, Yannick Goulam for technical support with our custom-built microscope, and Patrick J. Drew and Pablo Blinder for fruitful discussions. A.-K.A. would like to thank Alexandra Elbakyan for her hard work in extending scientific knowledge for all, without physical or financial boundaries. Financial support was provided by the Institut National de la Santé et de la Recherche Médicale (INSERM), the European Research Council (ERC-2013-AD6; 339513), the Fondation pour la Recherche Médicale (EQU201903007811), the Agence Nationale de la Recherche (NR-16-RHUS-0004 [RHU TRT_cSVD]), the Fondation Leducq Transatlantic Networks of Excellence program (16CVD05, Understanding the role of the perivascular space in cerebral small vessel disease), and the Institut Hospitalo-Universitaire FOReSIGHT (ANR-18-IAHU-0001) supported by French state funds managed by the Agence Nationale de la Recherche within the Investissements d'Avenir program.

1. C. Iadecola, The neurovascular unit coming of age: A journey through neurovascular coupling in health and disease. *Neuron* **96**, 17–42 (2017).
2. L. Kaplan, B. W. Chow, C. Gu, Neuronal regulation of the blood-brain barrier and neurovascular coupling. *Nat. Rev. Neurosci.* **21**, 416–432 (2020).
3. C. Iadecola, G. Yang, T. J. Ebner, G. Chen, Local and propagated vascular responses evoked by focal synaptic activity in cerebellar cortex. *J. Neurophysiol.* **78**, 651–659 (1997).
4. B. R. Chen, M. G. Kozberg, M. B. Bouchard, M. A. Shaik, E. M. C. Hillman, A critical role for the vascular endothelium in functional neurovascular coupling in the brain. *J. Am. Heart Assoc.* **3**, e000787 (2014).
5. T. A. Longden *et al.*, Capillary K^+-sensing initiates retrograde hyperpolarization to increase local cerebral blood flow. *Nat. Neurosci.* **20**, 717–726 (2017).
6. R. L. Rungta, E. Chaigneau, B.-F. Osmanski, S. Charpak, Vascular compartmentalization of functional hyperemia from the synapse to the pia. *Neuron* **99**, 362–375.e4 (2018).
7. R. L. Rungta *et al.*, Diversity of neurovascular coupling dynamics along vascular arbors in layer II/III somatosensory cortex. *Commun. Biol.* **4**, 855 (2021).
8. P. O'Herron *et al.*, Neural correlates of single-vessel haemodynamic responses in vivo. *Nature* **534**, 378–382 (2016).
9. D. Malonek, A. Grinvald, Interactions between electrical activity and cortical microcirculation revealed by imaging spectroscopy: Implications for functional brain mapping. *Science* **272**, 551–554 (1996).
10. I. Vanzetta, A. Grinvald, Increased cortical oxidative metabolism due to sensory stimulation: Implications for functional brain imaging. *Science* **286**, 1555–1558 (1999).

11. U. Lindauer *et al.*, No evidence for early decrease in blood oxygenation in rat whisker cortex in response to functional activation. *Neuroimage* **13**, 988–1001 (2001).
12. A. K. Dunn, A. Devor, A. M. Dale, D. A. Boas, Spatial extent of oxygen metabolism and hemodynamic changes during functional activation of the rat somatosensory cortex. *Neuroimage* **27**, 279–290 (2005).
13. Y. B. Sirotin, E. M. C. Hillman, C. Bordier, A. Das, Spatiotemporal precision and hemodynamic mechanism of optical point spreads in alert primates. *Proc. Natl. Acad. Sci. U.S.A.* **106**, 18390–18395 (2009).
14. Y. Ma *et al.*, Wide-field optical mapping of neural activity and brain haemodynamics: Considerations and novel approaches. *Philos. Trans. R. Soc. Lond. B Biol. Sci.* **371**, 20150360 (2016).
15. R. S. Menon *et al.*, BOLD based functional MRI at 4 Tesla includes a capillary bed contribution: Echo-planar imaging correlates with previous optical imaging using intrinsic signals. *Magn. Reson. Med.* **33**, 453–459 (1995).
16. X. Hu, T. H. Le, K. Uğurbil, Evaluation of the early response in fMRI in individual subjects using short stimulus duration. *Magn. Reson. Med.* **37**, 877–884 (1997).
17. E. Yacoub, X. Hu, Detection of the early negative response in fMRI at 1.5 Tesla. *Magn. Reson. Med.* **41**, 1088–1092 (1999).
18. B. Yeşilyurt, K. Uğurbil, K. Uludağ, Dynamics and nonlinearities of the BOLD response at very short stimulus durations. *Magn. Reson. Imaging* **26**, 853–862 (2008).
19. N. K. Logothetis, H. Guggenberger, S. Peled, J. Pauls, Functional imaging of the monkey brain. *Nat. Neurosci.* **2**, 555–562 (1999).
20. D.-S. Kim, T. Q. Duong, S.-G. Kim, High-resolution mapping of iso-orientation columns by fMRI. *Nat. Neurosci.* **3**, 164–169 (2000).
21. R. B. Buxton, The elusive initial dip. *Neuroimage* **13**, 953–958 (2001).
22. I. Vanzetta, A. Grinvald, Evidence and lack of evidence for the initial dip in the anesthetized rat: Implications for human functional brain imaging. *Neuroimage* **13**, 959–967 (2001).
23. X. Hu, E. Yacoub, The story of the initial dip in fMRI. *Neuroimage* **62**, 1103–1108 (2012).
24. K. Uludağ, P. Blinder, Linking brain vascular physiology to hemodynamic response in ultra-high field MRI. *Neuroimage* **168**, 279–295 (2018).
25. K.-S. Hong, A. Zafar, Existence of initial dip for BCI: An illusion or reality. *Front. Neurorobot.* **12**, 69 (2018).
26. J. K. Thompson, M. R. Peterson, R. D. Freeman, Single-neuron activity and tissue oxygenation in the cerebral cortex. *Science* **299**, 1070–1072 (2003).
27. J. Lecoq *et al.*, Odor-evoked oxygen consumption by action potential and synaptic transmission in the olfactory bulb. *J. Neurosci.* **29**, 1424–1433 (2009).
28. J. Lecoq *et al.*, Simultaneous two-photon imaging of oxygen and blood flow in deep cerebral vessels. *Nat. Med.* **17**, 893–898 (2011).
29. A. Parpaleix, Y. Goulam Houssen, S. Charpak, Imaging local neuronal activity by monitoring PO_2 transients in capillaries. *Nat. Med.* **19**, 241–246 (2013).
30. K. Masamoto, I. Kanno, Anesthesia and the quantitative evaluation of neurovascular coupling. *J. Cereb. Blood Flow Metab.* **32**, 1233–1247 (2012).
31. M. A. Pisauro, N. T. Dhruv, M. Carandini, A. Benucci, Fast hemodynamic responses in the visual cortex of the awake mouse. *J. Neurosci.* **33**, 18343–18351 (2013).
32. T. V. Esipova *et al.*, Oxyphor 2P: A high-performance probe for deep-tissue longitudinal oxygen imaging. *Cell Metab.* **29**, 736–744.e7 (2019).
33. M. Roche *et al.*, In vivo imaging with a water immersion objective affects brain temperature, blood flow and oxygenation. *eLife* **8**, e47324 (2019).
34. M. Li, P. Miao, Y. Zhu, S. Tong, Functional laser speckle imaging of cerebral blood flow under hypothermia. *J. Biomed. Opt.* **16**, 086011 (2011).
35. M. Smear, A. Resulaj, J. Zhang, T. Bozza, D. Rinberg, Multiple perceptible signals from a single olfactory glomerulus. *Nat. Neurosci.* **16**, 1687–1691 (2013).
36. N. Jukovskaya, P. Tiret, J. Lecoq, S. Charpak, What does local functional hyperemia tell about local neuronal activation? *J. Neurosci.* **31**, 1579–1582 (2011).
37. E. Chaigneau, A. J. Wright, S. P. Poland, J. M. Girkin, R. A. Silver, Impact of wavefront distortion and scattering on 2-photon microscopy in mammalian brain tissue. *Opt. Express* **19**, 22755–22774 (2011).
38. D. G. Lyons, A. Parpaleix, M. Roche, S. Charpak, Mapping oxygen concentration in the awake mouse brain. *eLife* **5**, e12024 (2016).
39. M. Wachowiak, L. B. Cohen, Representation of odorants by receptor neuron input to the mouse olfactory bulb. *Neuron* **32**, 723–735 (2001).
40. K. M. Sicard, T. Q. Duong, Effects of hypoxia, hyperoxia, and hypercapnia on baseline and stimulus-evoked BOLD, CBF, and CMRO2 in spontaneously breathing animals. *Neuroimage* **25**, 850–858 (2005).
41. A. Sumiyoshi *et al.*, Coupling between gamma oscillation and fMRI signal in the rat somatosensory cortex: Its dependence on systemic physiological parameters. *Neuroimage* **60**, 738–746 (2012).
42. G. M. Rossetti *et al.*, Reversal of neurovascular coupling in the default mode network: Evidence from hypoxia. *J. Cereb. Blood Flow Metab.* **41**, 805–818 (2021).
43. B. M. Ances, D. G. Buerk, J. H. Greenberg, J. A. Detre, Temporal dynamics of the partial pressure of brain tissue oxygen during functional forepaw stimulation in rats. *Neurosci. Lett.* **306**, 106–110 (2001).
44. K. Masamoto *et al.*, Biphasic changes in tissue partial pressure of oxygen closely related to localized neural activity in guinea pig auditory cortex. *J. Cereb. Blood Flow Metab.* **23**, 1075–1084 (2003).
45. H. S. Wei *et al.*, Erythrocytes are oxygen-sensing regulators of the cerebral microcirculation. *Neuron* **91**, 851–862 (2016).
46. M. B. Richard, S. R. Taylor, C. A. Greer, Age-induced disruption of selective olfactory bulb synaptic circuits. *Proc. Natl. Acad. Sci. U.S.A.* **107**, 15613–15618 (2010).
47. M. Watanabe, A. Bartels, J. H. Macke, Y. Murayama, N. K. Logothetis, Temporal jitter of the BOLD signal reveals a reliable initial dip and improved spatial resolution. *Curr. Biol.* **23**, 2146–2150 (2013).
48. K. Uludağ, B. Müller-Bierl, K. Uğurbil, An integrative model for neuronal activity-induced signal changes for gradient and spin echo functional imaging. *Neuroimage* **48**, 150–165 (2009).
49. A. C. Silva, S.-P. Lee, C. Iadecola, S.-G. Kim, Early temporal characteristics of cerebral blood flow and deoxyhemoglobin changes during somatosensory stimulation. *J. Cereb. Blood Flow Metab.* **20**, 201–206 (2000).
50. C. Martin, J. Martindale, J. Berwick, J. Mayhew, Investigating neural-hemodynamic coupling and the hemodynamic response function in the awake rat. *Neuroimage* **32**, 33–48 (2006).
51. İ. Şencan *et al.*, Optical measurement of microvascular oxygenation and blood flow responses in awake mouse cortex during functional activation. *J. Cereb. Blood Flow Metab.* **42**, 510–525 (2022).
52. H. Dana *et al.*, Thy1-GCaMP6 transgenic mice for neuronal population imaging in vivo. *PLoS One* **9**, e108697 (2014).
53. T. V. Esipova *et al.*, Two new "protected" oxyphors for biological oximetry: Properties and application in tumor imaging. *Anal. Chem.* **83**, 8756–8765 (2011).
54. A.-K. Aydin *et al.*, Transfer functions linking neural calcium to single voxel functional ultrasound signal. *Nat. Commun.* **11**, 2954 (2020).
55. D. Boido *et al.*, Mesoscopic and microscopic imaging of sensory responses in the same animal. *Nat. Commun.* **10**, 1110 (2019).
56. E. Chaigneau *et al.*, The relationship between blood flow and neuronal activity in the rodent olfactory bulb. *J. Neurosci.* **27**, 6452–6460 (2007).
57. A.-K. Aydin, C. Verdier, S. Charpak, The oxygen initial dip in the brain of anesthetized and awake mice. Zenodo. https://doi.org/10.5281/zenodo.5804933. Deposited 26 December 2021.
58. A.-K. Aydin, C. Verdier, S. Charpak, InitialDip_AydinEtAl. GitHub. https://github.com/alike-aydin/InitialDip_AydinEtAl. Deposited 22 February 2022.